FIRE AND MATERIALS
*Fire Mater.* 2003; **27**:209–222 (DOI: 10.1002/fam.822)

# Radiative heat flux measurement uncertainty

Rodney Bryant[1,*,†], Carole Womeldorf[2], Erik Johnsson[1] and Thomas Ohlemiller[1]

[1] *Building and Fire Research Laboratory, National Institute of Standards and Technology, 100 Bureau Drive, MS 8662, Gaithersburg, MD 20899, U.S.A.*
[2] *Department of Mechanical Engineering, Johns Hopkins University, Baltimore, MD 21218, U.S.A.*

## SUMMARY

As part of an effort to characterize the uncertainties associated with heat flux measurements in a fire environment, an uncertainty analysis example was performed using measurement data from a room corner surface products test that followed the guidelines of ISO 9705. Equations to model the heat transfer at the surface of a Schmidt-Boelter (thermopile) type total heat flux gauge were selected for use to calculate the incident radiative flux from a total heat flux measurement. The effects of the heat flux measurement uncertainty sources were evaluated by conducting an uncertainty propagation on the resulting equation for incident radiation. For the model equations and the example conditions selected, the free-stream temperature estimate and the heat flux gauge calibration constant were determined to be major uncertainty contributors. The study demonstrates how to systematically identify major sources of uncertainty for the purpose of reducing total uncertainty and thereby enhancing experiment design. Published in 2003 by John Wiley & Sons, Ltd.

KEY WORDS: uncertainty analysis; heat transfer; heat flux gauge

## 1. INTRODUCTION

Heat can be transmitted by three modes: convection, conduction and radiation. Total heat flux gauges are non-ideal and can have responses that are sensitive to each mode. Radiation is a significant mode of heat transfer in typical fire environments; it is particularly important to enclosure fires where its cumulative pre-heating effects accelerate burning and increase the chances of flashover. Though the incident radiation is independent of the heat flux gauge measurement, interpretation of the measurement may require knowledge of several parameters. Consequently, the uncertainty associated with a heat flux measurement depends on multiple factors such as the gauge characteristics, the calibration conditions and accuracy, as well as the incident flux modes and magnitudes in the actual measurement situation [1,2].

Total heat flux gauges are typically employed in fire test measurements. The gauges measure the combined effects of radiation and convection. Therefore, the convective component contributes to the total uncertainty when radiation is the quantity required. Total heat flux

*Correspondence to: R. Bryant, NIST, 100 Bureau Drive, M.S. 8662, Gaithersburg, MD 20899, U.S.A.
†E-mail: rbryant@nist.gov



*Received 4 April 2003*
*Accepted 20 May 2003*

gauges can be configured with glass windows to minimize the convective effects, however, additional influences and uncertainties are introduced by the optical properties of the glass. Investigations by Robertson and Ohlemiller [3] and Wetterlund and Persson [4] demonstrate methods to quantify the convective component for some specific total heat flux measurements. Approximately 25% uncertainty for methods to partition the heat flux measurement was reported in both investigations.

It is often the case that a physical quantity of interest cannot be measured in a single direct measurement but is instead determined over multiple steps. One or more quantities are measured directly, and the quantity of interest is calculated from them. When a measurement requires multiple steps, the estimation of uncertainty must account for each step. The uncertainties of the direct measurements must be estimated and then it must be determined how each uncertainty propagates through to the final quantity of interest [5]. The physical quantity of interest for this study is incident radiative flux. There exist several types of heat flux gauges capable of responding to the incident radiative flux; for this study only the Schmidt-Boelter total heat flux gauge will be considered. Neither total heat flux nor incident radiative flux can be measured directly. Both require indirect measurements, therefore an uncertainty propagation is required to estimate the total measurement uncertainty.

The purpose of the present study was to develop a better understanding of the uncertainties associated with heat flux measurements. Radiant heat flux was selected as the mode of heat transfer for study due to its role in the evaluation of potential fire growth. Equations were selected from the literature to represent the radiative flux incident on a heat flux gauge, and data from a standard fire test were selected to illustrate the partitioning of a total heat flux measurement. Finally, an uncertainty propagation was performed to estimate the combined uncertainty of the calculation of incident radiative flux.

## 2. MODEL EQUATIONS

For the experimental arrangement to be analysed here, the heat flux gauge was free standing above the floor and located in the geometric center of the room as described in the details of ISO 9705 [6]. The gauge views radiation from the surroundings and is subject to convection from a cross flow in the lower layer of the room as displayed in Figure 1. The cross flow is due to the inflow of air from a doorway located along one wall of the room. A control volume may be defined to encompass the top surface of the gauge. At this surface, the first law of thermodynamics requires the energy entering and leaving the surface to balance. This requirement is exploited to determine indirectly the mode of heat transfer under study, i.e. the incident radiative flux ($q''_{\mathrm{rad,\,inc}}$).

The gauges required for ISO 9705 are either Gardon (foil) or Schmidt-Boelter (thermopile) type. Both gauge types respond to radiation and convection, though to varying degrees. The response of the Gardon gauge may be nonlinear when subject to mixed mode heat transfer [7]. The description of heat transfer for the Schmidt-Boelter gauge is simpler and it was therefore selected for this study. The Schmidt-Boelter gauge consists of a thin insulating material across which a temperature difference is measured by use of a thermopile or series arrangement of tiny thermocouple junctions. The thermopile is useful for creating a substantial voltage output for a small temperature difference [8,9].

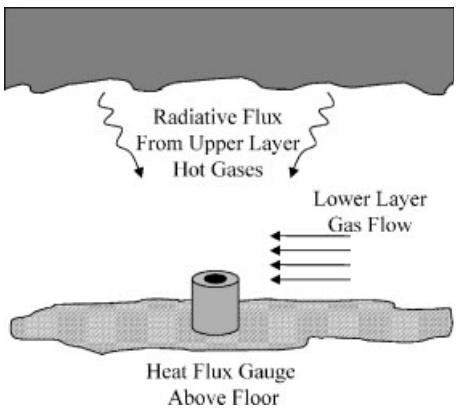


Figure 1. Total heat flux gauge setup for the room corner surface products test.

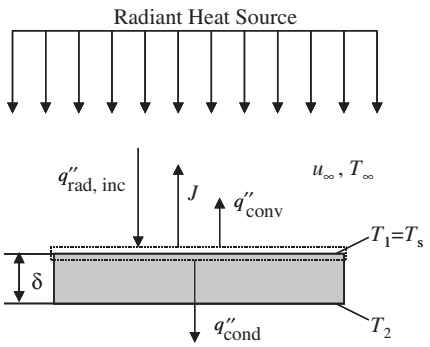


Figure 2. Energy balance at heat flux gauge surface.

### 2.1. *Energy balance*

Figure 2 displays the control volume encompassing the sensor surface of the Schmidt-Boelter heat flux gauge, which is subject to radiative heat transfer due to a radiant source and convection due to a cross flow at free-stream velocity and temperature, $u_\infty$ and $T_\infty$, respectively. Radiation from the surroundings enters the control volume and therefore impinges upon the sensor surface. The majority of the radiation is absorbed into the surface, however, a small portion is reflected away from the surface and exits the control volume. In addition the surface emits radiation through the control volume to the surroundings. In this example, heat flow due to convection and conduction is away from the surface and therefore exits the control volume. Convective heat flow can be into or out of the sensor surface, as defined by the greater of the surface or free-stream temperature. The direction here is arbitrarily selected as out of the surface.

Assuming steady-state heat transfer, Arai *et al.* [10] have described the balance of heat into and away from the control volume by Equations (1) and (2),

$$q''_{\text{rad, inc}} = J + q''_{\text{conv}} + q''_{\text{cond}} \tag{1}$$

where

$$J = (1 - \varepsilon_s) q''_{\text{rad, inc}} + \varepsilon_s \sigma T_s^4 \tag{2}$$

is the combination of radiation reflected and emitted from a surface at temperature, $T_s$. The surface is assumed to be diffuse and gray, therefore the surface emissivity, $\varepsilon_s$, and absorptivity are the same. A typical commercial heat flux gauge measures the heat conducted away from its surface by measuring the temperature gradient through the surface material. The mode of heat transfer under study, incident radiation, can therefore be calculated using Equation (1) with knowledge of the parameters required to estimate the convective heat transfer.

### *2.2. Convection estimate*

The heat flux gauge standing above the floor is analogous to a finite cylinder protruding into a cross-flow. Practical analysis of the heat transfer to such a shape suggests that it should be treated in two parts: for the heat transfer to the sides, estimates for an infinite circular cylinder are applied; for the heat transfer to the top or end surface, estimates for a flat plate are applied. Because the gauge sensor is located on the top surface, as shown in Figure 1, it is this surface that will be considered in the present analysis.

Treating the top surface as a flat plate is a reasonable first order estimate [11], however, the flow over the top surface is more complex than a typical flat plate boundary layer flow. Tsutsui *et al.* [12] conducted experiments on a scale model of an oil storage tank in both laminar and turbulent cross flows to measure the convective heat transfer coefficients for the sides, roof and overall shape. The scale model of the tank was a finite circular cylinder similar to the heat flux gauge above the floor. The result of Tsutsui *et al.* for the top-surface average heat transfer coefficient, $h_{\text{avg}}$, is applied in the present study, Equation (3). The Reynolds number, calculated based on the diameter, $d$, of the gauge, is approximately 2200 for the flow conditions under study. Therefore the flow across the gauge is assumed to be laminar and it is appropriate to employ the average heat transfer coefficient in the convection estimate [13]. The following equation estimates the convective heat flux at the gauge surface.

$$q''_{\text{conv}} = h_{\text{avg}}(T_s - T_\infty) = \frac{0.24 u_\infty^{2/3} k_g}{\nu^{2/3} d^{1/3}} (T_s - T_\infty) \tag{3}$$

Because the gauge is located in the lower layer of the room, it is subject to the air flowing into the enclosure during the fire test. Therefore the fluid properties, thermal conductivity, $k_g$, and kinematic viscosity, $\nu$, are calculated for air at the film temperature for the gauge surface, $T_f = (T_s + T_\infty)/2$.

### *2.3. Calibration relation*

Heat flux gauges are typically calibrated with a radiant source, usually a blackbody furnace, traceable to a temperature standard. The result of the calibration is typically a linear relation, Equation (4), between the heat flux gauge output voltage, $V_{\text{sensor}}$, and the incident radiation from the radiant source. The gauge manufacturer supplies the calibration constant, $C_{\text{sensor}}$. Typical

commercial gauges measure the conductive heat flux at the surface, $q''_{\text{cond}}$. Therefore the energy balance across the surface in Figure 2 can be applied again, but for the case of a calibration with a radiant source. Convective effects during the calibration are usually assumed to be negligible. This assumption is currently debated and its impact is not yet clear, however, it shall be adopted for the sake of clarity of the illustration being presented. Similarly, the radiation emitted from the gauge surface is assumed to be negligible for mid range radiation calibrations [14]. However, the $T_s^4$ term will be included for the purposes of this study due to the current ability of gauges to record their surface temperature. It may not be practical to match or maintain the gauge surface temperature during actual use at the surface temperature during calibration, therefore the additional subscript of 'cal' is added. Equation (5) represents the energy balance during calibration with a radiant source and negligible convection effects. Equation (4) can be substituted for incident radiation to form Equation (6), the relation between the actual gauge measurement, conduction, and the calibration results.

$$q''_{\text{rad, inc, cal}} = C_{\text{sensor}} V_{\text{sensor}} \tag{4}$$

$$q''_{\text{cond}} = \varepsilon_s q''_{\text{rad, inc, cal}} - \varepsilon_s \sigma T^4_{\text{s, cal}} \tag{5}$$

$$q''_{\text{cond}} = \varepsilon_s C_{\text{sensor}} V_{\text{sensor}} - \varepsilon_s \sigma T^4_{\text{s, cal}} \tag{6}$$

### 2.4. Incident radiation

Combining Equations (1), (2), (3) and (6) completes the expression for the calculation of incident radiation from a total heat flux gauge measurement and is given by

$$q''_{\text{rad, inc}} = \frac{1}{\varepsilon_s}\left[\frac{0.24 u_\infty^{2/3} k_g}{\nu^{2/3} d^{1/3}}(T_s - T_\infty) + \varepsilon_s \sigma (T_s^4 - T^4_{\text{s, cal}}) + \varepsilon_s C_{\text{sensor}} V_{\text{sensor}}\right] \tag{7}$$

The uncertainty of the voltage measurement, calibration constant and the estimates of the flow temperature and velocity and relevant fluid properties will determine the uncertainty of the incident radiation measurement. Equation (7) represents an attempt to calculate the incident radiation from total heat flux gauge measurements. The uncertainty of the inferred incident radiation can be estimated by applying an uncertainty propagation to this relation.

## 3. UNCERTAINTY ANALYSIS

Suppose a set of measurements is made to determine the result, $R$. The result can be expressed as a function of the independent variables, some of which are the direct measurements.

$$R = R(x_1, x_2, x_3, \ldots, x_n) \tag{8}$$

If the uncertainties of the independent variables are uncorrelated, the combined relative uncertainty of the result, $R$, is given by Equation (9) [5,9,15].

$$\frac{w_R}{R} = \left[\left(s_1 \frac{w_1}{x_1}\right)^2 + \left(s_2 \frac{w_2}{x_2}\right)^2 + \cdots + \left(s_N \frac{w_N}{x_N}\right)^2\right]^{1/2} \tag{9}$$

$$s_i = \frac{\partial R}{\partial x_i}\frac{x_i}{R} \tag{10}$$

In Equation (9), $w_i$ is the standard uncertainty of each input parameter and $s_i$ is the non-dimensional sensitivity coefficient given by Equation (10). The sensitivity coefficients determine the contribution of uncertainty for their associated variable to the combined uncertainty. An uncertainty propagation, as described by Equation (9), is very useful in experimental design to isolate variables that are significant contributors to the overall uncertainty of the desired result.

The result under study, incident radiative flux, has been expressed as a function of several variables, all of which are assumed to be independent with uncorrelated individual uncertainties. Several of the variables, such as gauge output voltage, surface temperature, free-stream temperature and velocity, can be measured directly. Other variables are given as constants or are estimated from reference tables.

Applying Equation (7) to Equation (9), the general expression for the combined relative uncertainty of the incident radiative flux measurement is

$$\frac{w_{q''_{\text{rad, inc}}}}{q''_{\text{rad, inc}}} = \left[ \begin{array}{l} \left(s_{\varepsilon_s}\dfrac{w_{\varepsilon_s}}{\varepsilon_s}\right)^2 + \left(s_{C_{\text{sensor}}}\dfrac{w_{C_{\text{sensor}}}}{C_{\text{sensor}}}\right)^2 + \left(s_{V_{\text{sensor}}}\dfrac{w_{V_{\text{sensor}}}}{V_{\text{sensor}}}\right)^2 \\ \quad + \left(s_{T_{\text{s, cal}}}\dfrac{w_{T_{\text{s, cal}}}}{T_{\text{s, cal}}}\right)^2 + \left(s_{T_s}\dfrac{w_{T_s}}{T_s}\right)^2 + \left(s_{u_\infty}\dfrac{w_{u_\infty}}{u_\infty}\right)^2 \\ \quad + \left(s_{T_\infty}\dfrac{w_{T_\infty}}{T_\infty}\right)^2 \end{array} \right]^{1/2} \tag{11}$$

Both the gas conductivity and kinematic viscosity are functions of gas temperature, and the tabulated data can be expressed as polynomial fits. Therefore both gas properties are entered into Equation (7) as expressions of the film temperature and their partial derivative is computed with respect to the surface and free-stream temperature. Equations (12)–(18) represent the partial derivative terms of the sensitivity coefficients. Note that the full differentiation of the gas property relations for gas conductivity and kinematic viscosity are not printed in Equations (16) and (18) for brevity.

$$\frac{\partial q''_{\text{rad, inc}}}{\partial \varepsilon_s} = \frac{-0.24 u_\infty^{2/3} k_g (T_s - T_\infty)}{\varepsilon_s^2 d^{1/3} \nu^{2/3}} \tag{12}$$

$$\frac{\partial q''_{\text{rad, inc}}}{\partial C_{\text{sensor}}} = V_{\text{sensor}} \tag{13}$$

$$\frac{\partial q''_{\text{rad, inc}}}{\partial V_{\text{sensor}}} = C_{\text{sensor}} \tag{14}$$

$$\frac{\partial q''_{\text{rad, inc}}}{\partial T_{\text{s, cal}}} = -4\sigma T_{\text{s, cal}}^3 \tag{15}$$

$$\frac{\partial q''_{\text{rad, inc}}}{\partial T_s} = \frac{0.24 u_\infty^{2/3}}{\varepsilon_s d^{1/3} \nu^{2/3}} \left[ k_g + \frac{\partial k_g}{\partial T_s}(T_s - T_\infty) - \frac{2k_g}{3\nu}\frac{\partial \nu}{\partial T_s}(T_s - T_\infty) \right] + 4\sigma T_s^3 \tag{16}$$

$$\frac{\partial q''_{\text{rad, inc}}}{\partial u_\infty} = \frac{0.16 k_g (T_s - T_\infty)}{\varepsilon_s d^{1/3} u_\infty^{1/3} \nu^{2/3}} \tag{17}$$

$$\frac{\partial q''_{\text{rad, inc}}}{\partial T_\infty} = \frac{0.24 u_\infty^{2/3}}{\varepsilon_s d^{1/3} \nu^{2/3}} \left[ \frac{\partial k_g}{\partial T_\infty} (T_s - T_\infty) - k_g - \frac{2 k_g}{3\nu} \frac{\partial \nu}{\partial T_\infty} (T_s - T_\infty) \right] \tag{18}$$

## 4. APPLICATION EXAMPLE

The ISO 9705—Full-Scale Room Test for Surface Products—is designed to evaluate the contribution to fire growth by wall or ceiling surface products [6]. Several principal measurements, such as total heat flux, total heat release rate, gas composition and optical density, may be conducted to evaluate the potential hazards of the fire. The measurement of interest for this study is total heat flux. By measuring total heat flux incident on a heat flux gauge at the center of the floor, the test provides a measure of the potential for fire spread to other objects within the room, but remote from the ignition source. The standard recognizes that the total heat flux measurement consists of heat transfer contributions from both radiation and convection with the major component being radiation. The standard also suggests, but does not require, measurements of gas temperature in the room and velocity through the doorway if additional information is required. For the present study, gas temperature and velocity measurements are necessary for estimating the convective heat transfer. For the reasons mentioned, heat flux measurements from the ISO 9705 or similar tests serve as excellent examples of fire-environment total heat flux measurements with existing potential for partitioning of the modes of heat transfer.

A series of large-scale room fire experiments was conducted at the Technical Research Centre of Finland [16]. The test room had six times more surface area than a similar room required by ISO 9705. The purpose of the tests was to compare the performance of surface products with their performance in smaller scale tests, specifically ISO 9705. Because the tests followed the procedure of ISO 9705 as much as possible they were selected as an appropriate source of data for this study. The data were used to illustrate the calculation of incident radiative flux from the total heat flux measurement, Equation (7), and to estimate the uncertainty of the calculation using Equation (11). Measurement data of total heat flux at the floor, lower layer gas temperature at the doorway and lower layer velocity at the doorway serve as input for the calculation. The surface product test selected, a combustible facing on mineral wool, demonstrated total floor heat fluxes ranging from low levels to heat flux levels typical of flashover conditions.

Estimates of the input parameters for Equation (7) and their uncertainties are listed in Table I. Variables are taken directly from the product test data or inferred directly from the data as in the case of the gauge output voltage. Estimated values for the gauge surface emissivity and the gauge calibration constant were assumed from manufacturer specifications. Estimated values for the gauge surface temperature and the gauge diameter were assumed from the requirements of ISO 9705. Though not stated in ISO 9705, it was assumed that each uncertainty estimate was modeled by a normal probability distribution and represents a 67% probability that the parameter value lies in the interval $w_{i,-}$ to $w_{i,+}$. Similar assumptions were made for the remaining uncertainty estimates. Because the parameter uncertainty estimates are based on

Table I. Input parameter and uncertainty estimates.

| Parameter | Value | Relative uncertainty |
|---|---|---|
| $\varepsilon_s$ | 0.96* | 3.0%* |
| $C_{sensor}$ | 5132 W/(m$^2$ mV)* | 3.0%* |
| $V_{sensor}$ | −0.02 mV to 4.07 mV† | 0.5%† |
| $T_{s,\,cal}$ | 295 K§ | 1.0%§ |
| $T_s$ | 297 K† | 2.0%† |
| $u_\infty$ | 0.3 m/s to 1.3 m/s† | 20%† |
| $T_\infty$ | 289 K to 337 K† | 10%‡ |
| $d$ | 0.025 m† | — |

*Manufacturer specifications.
†ISO 9705.
‡Blevins and Pitts [18].
§General knowledge.

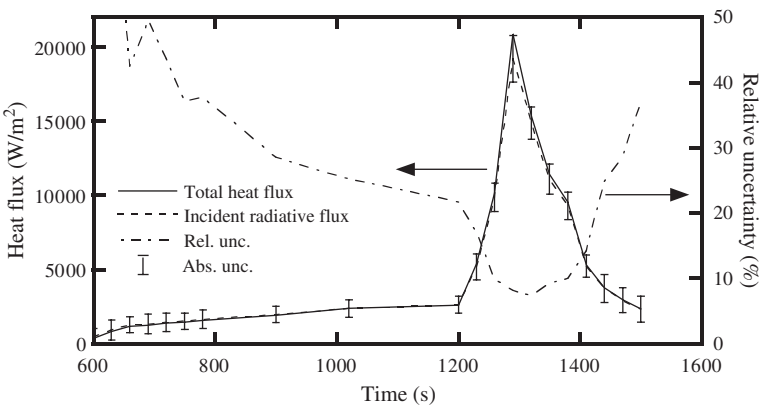


Figure 3. Total heat flux measurements taken from a room corner surface products test, the calculated incident radiative flux and its estimated combined relative uncertainty.

manufacturer's specifications, data from reports, or general knowledge, they are classified as type B uncertainties [17]. The estimates of uncertainty listed in Table I are established as a baseline. All uncertainties reported are standard uncertainties, $w_i = \sigma_i$.

It is important to note that the data of lower layer temperature and velocity measurements at the doorway serve as estimates for the free-stream temperature and free-stream velocity near the heat flux gauge. Such estimates are required for the calculation of convective heat flux, Equation (3). Since actual measurements of free-stream temperature and velocity near the gauge are not available, the reader is reminded that the analysis is an approximation of radiative heat flux and an illustration of the process of uncertainty propagation.

Figure 3 demonstrates the time history of both the measured total heat flux and the calculated incident radiative flux from Equation (7) on the primary $y$-axis. The combined absolute uncertainty is displayed as error bars on the flux curve while the combined relative uncertainty is displayed on the secondary $y$-axis. Only results at times greater than 600 s are displayed because

the heat flux levels prior to this period are small and sometimes negative due to cooling of the heat flux gauge by the cross flow. The average percent difference between the total heat flux measured and the calculated incident radiative flux is 4.6%. This agrees with ISO 9705, which assumes radiation to be the main component of the total heat flux measurement. The estimated combined relative uncertainty of the calculation of incident radiative flux is 25% or greater for total heat flux measurements below 2400 $W/m^2$. For higher total heat flux measurements the estimated combined relative uncertainty ranges from 7% to 29%, with less relative uncertainty at the higher heat flux.

Figure 4 displays again the estimated combined relative uncertainty of the calculated incident radiative flux. In addition, the relative uncertainty attributed to the individual parameters is displayed, as inferred from Equation (11). Because the combined relative uncertainty varies as the root mean square of the individual uncertainties, parameters with the largest uncertainty and a sensitivity coefficient greater than or approximately unity will produce the most significant contribution to the combined total. The uncertainty of the free-stream temperature measurement, the gauge surface temperature measurement and the calibration constant are the most significant contributors to the estimated combined relative uncertainty. The remaining parameters' uncertainties are relatively constant and insignificant over the test conditions. For heat flux levels below 5000 $W/m^2$, the order of the uncertainty contribution from the top three sources is: (1) the free-stream temperature measurement, (2) the gauge surface temperature measurement, and (3) the calibration constant. Near peak total heat flux, the uncertainty contribution from the calibration constant replaces the gauge surface temperature measurement as the second highest contributor and demonstrates a potential to compete with the free-stream temperature measurement as the highest contributor of uncertainty. To reduce the overall estimated uncertainty for situations similar to this test case, efforts should focus on reducing the uncertainty of the free-stream temperature measurement and the calibration constant.

Because the measurements considered in this example are dynamic, ranges and mean values of the ranges for the non-dimensional sensitivity coefficients are presented in Table II. Prior to flashover (600–1020 s), the gauge calibration factor, surface temperature at calibration, surface

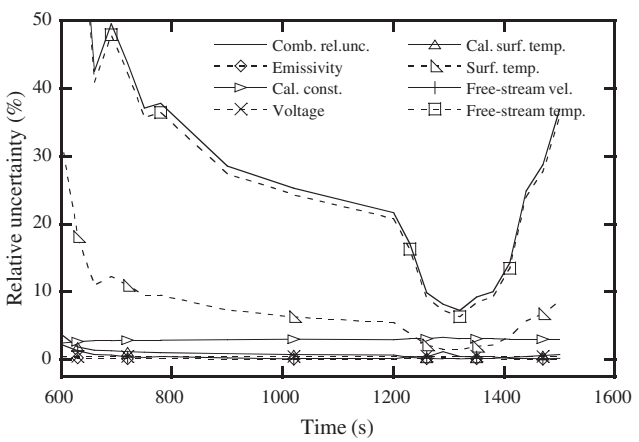


Figure 4. Combined relative uncertainty and the parameter uncertainty contribution.

Table II. Non-dimensional sensitivity coefficients.

| | $<2400$ W/m$^2$ 600 s to 1020 s | | $>2400$ W/m$^2$ 1200 s to 1470 s | |
|---|---|---|---|---|
| | Range | Mean | Range | Mean |
| $x_i$ | $s_i$ | $s_i$ | $s_i$ | $s_i$ |
| $\varepsilon_s$ | −0.17 to 0.01 | −0.05 | −0.01 to 0.09 | 0.03 |
| $C_{sensor}$ | 0.81 to 1.00 | 0.94 | 0.99 to 1.09 | 1.03 |
| $V_{sensor}$ | 0.81 to 1.00 | 0.94 | 0.99 to 1.09 | 1.03 |
| $T_{s,cal}$ | −3.75 to −0.72 | −1.47 | −0.66 to −0.09 | −0.31 |
| $T_s$ | 3.17 to 16.2 | 6.52 | 0.73 to 3.37 | 1.73 |
| $u_\infty$ | −0.01 to 0.11 | 0.04 | −0.06 to 0.01 | −0.02 |
| $T_\infty$ | −12.2 to −2.43 | −4.98 | −2.78 to −0.63 | −1.43 |

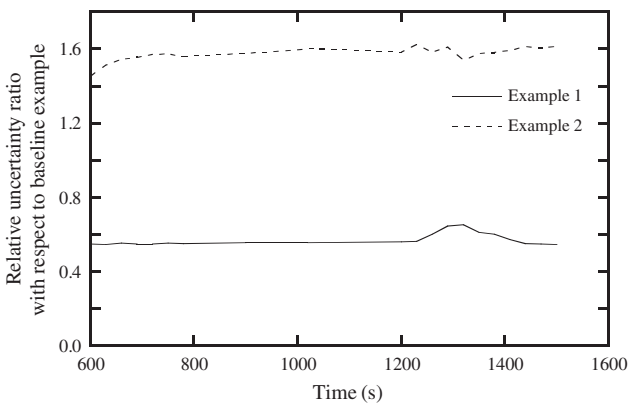


Figure 5. Effects of reducing parameter uncertainty and parameter constants. Baseline: $w_{T\infty} = 0.10T_\infty$, $d = 0.025$ m, Example 1: $w_{T\infty} = 0.05T_\infty$, $d = 0.025$ m, Example 2: $w_{T\infty} = 0.10T_\infty$, $d = 0.006$ m.

temperature, and the free-stream temperature all have mean sensitivity coefficients near or above 1.0. In the flashover and flashover transition region (1200–1470 s), it is important to note that the mean sensitivity coefficients of the surface and free-stream temperature are reduced but still greater than 1.0. Because both parameters are found in the convection term of Equation (7), it is an indication that convection becomes less important in the flashover stage of the fire. However, it should not be ignored.

A further example of the effects of reducing the parameter uncertainty is demonstrated in Figure 5. The baseline case of parameter uncertainty and constant values (Table I), estimates the relative uncertainty of the free-stream temperature measurement at 10%. This estimate comes from a study to determine the error of aspirated thermocouple measurements in enclosure fires [18]. Reducing this uncertainty by a factor of 2 greatly reduces the combined uncertainty. Figure 5 displays the ratio of the new combined relative uncertainty to that of the baseline case. In Figure 5, Example 1 corresponds to the case of reducing the free-stream temperature uncertainty to 5%. The average ratio of the uncertainty over the duration of the test is 0.57, indicating that the combined uncertainty can be reduced by almost a factor of 1.8 by reducing

the uncertainty of a single dominating parameter. In the flashover region (1200–1470 s), the free-stream temperature uncertainty no longer dominates; it is second to the uncertainty of the calibration constant. Therefore the ratio is higher in this region of the graph due to the reduced effect of free-stream temperature uncertainty.

Changing the values of the constant input parameters, such as surface emissivity, calibration constant and calibration surface temperature, resulted in a negligible effect on the total relative uncertainty. However, changing the diameter of the heat flux gauge surface did result in notable effects. Figure 5, Example 2, displays the effect of decreasing the gauge surface diameter by a factor of 4. The combined relative uncertainty increases by a factor of 1.57. The reduced diameter causes the convection component to increase as demonstrated in Equation (3). Therefore the sensitivity coefficients originating from the convection term will also increase as indicated in the partial differentials, Equations (16) and (18). These results suggest that larger Schmidt-Boelter gauges will have less heat transfer contribution from convection and less total uncertainty, since the average boundary layer will be thicker.

The uncertainty of the measurement is not only influenced by the uncertainty of the individual measurement parameters but it is also influenced by the assumptions used to arrive at the equations for modeling the physical processes. Presented earlier were the steps to assemble a model of the incident radiative flux by considering the energy balance across the face of the gauge, Equation (7). Within the model equation are sub-models for the different modes of heat transfer. The convection sub-model, which is derived from empirical data, will depend on the geometrical shape of the surfaces to which it is applied.

In the present example the geometry of the heat flux gauge standing above the floor is similar to that of an infinite cylinder in a cross-flow, however, the gauge is a finite cylinder and the subject of interest is the heat flux at the top (flat) surface of the finite cylinder. This brings into consideration the geometry for flow over a flat plate. At issue also is whether or not the free stream flow is laminar or turbulent. In the absence of a more similar geometric configuration for which the convection heat transfer coefficient is known, the most appropriate of the two geometries mentioned would be chosen and the flow would be treated as either laminar or turbulent. Fortunately, a more appropriate model of convection heat transfer coefficient was available through the work of Tsutsui *et al*. [12]. However, it is a useful exercise to estimate the limits of uncertainty based on the available choices of convection coefficients.

The average convective heat transfer coefficient is directly proportional to the empirically determined average Nusselt number. Empirical results for average Nusselt number for four applicable geometries are listed in Table III. Nusselt number is computed based on a characteristic Reynolds number (with respect to gauge diameter) and Prandtl number defined by

Table III. Average Nusselt number and convective heat transfer coefficient for applicable geometries.

| Geometry | $Nu_{avg}$ | $h_{avg}$ W/(m$^2$ K) |
|---|---|---|
| Finite vertical cylinder, laminar | $0.24Re^{2/3}$ | 42.7 |
| Finite vertical cylinder, turbulent | $0.29Re^{2/3}$ | 51.6 |
| Infinite cylinder | $0.26Re^{0.6}Pr^{0.37}$ | 24.3 |
| Flat plate | $0.664Re^{1/2}Pr^{1/3}$ | 29.1 |
| | $Re = 2200$, $Pr = 0.7$, $k_g$ for air at 300 K<br>$h^*_{avg} = 36.9$ W/(m$^2$ K), $\sigma_{h^*_{avg}} = 12.5$ W/(m$^2$ K) | |

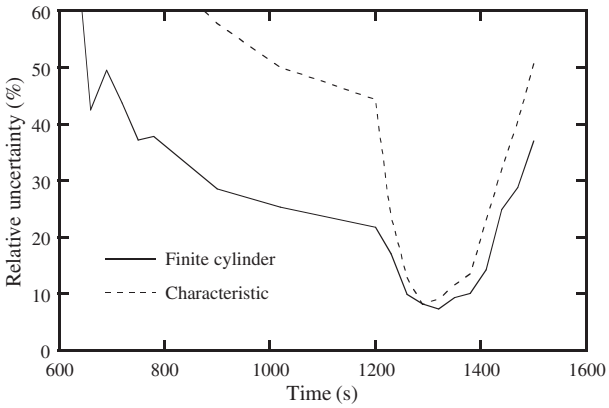


Figure 6. Combined relative uncertainty comparison for the two applications of heat transfer coefficient: laminar flow over a finite cylinder and a characteristic coefficient.

the conditions of the present example. From the four applicable heat transfer coefficients, the mean and standard deviation were computed and employed as a characteristic heat transfer coefficient and estimated uncertainty, respectively. The characteristic heat transfer coefficient, Equation (19), was used as input for Equation (3) and the uncertainty propagation was repeated with the new convection estimate and estimated uncertainty for the heat transfer coefficient.

$$h^*_{\text{avg}} = \frac{\sum_{i=1}^{N} h_{\text{avg},\,i}}{N} = \frac{\sum_{i=1}^{N} \frac{Nu_{\text{avg},\,i} k_g}{d}}{N} \tag{19}$$

Figure 6 displays the resulting combined relative uncertainty when a characteristic heat transfer coefficient is applied. The previous results for the specific case of flow over the top of a finite cylinder, is again presented for comparison. In the region near flashover, where radiation dominates, there is agreement in the estimates of uncertainty. However, in regions of low radiative flux the uncertainty is large for the case of the characteristic heat transfer coefficient. This example illustrates that the choice of the model for estimating the convective heat transfer is very important when the convection contribution is significant. In addition, it estimates bounding limits on the uncertainty in the region near flashover and increases confidence in applying the heat flux gauge in this configuration for high radiation flux conditions.

## 5. CONCLUSIONS

The present study illustrates a method to calculate incident radiative flux from a total heat flux measurement and subsequently how to estimate the combined uncertainty of the calculation by applying an uncertainty propagation. Data from a room corner surface products test, similar to the ISO 9705, were employed as an example to illustrate the incident radiative flux calculation and the uncertainty analysis. The analysis only approximated the incident radiative flux because required input parameters such as free-stream temperature and free-stream velocity near the heat flux gauge were estimated from measurements in the doorway. The convective heat transfer

correlation is also an approximation based on empirical results. However, the results demonstrated that radiative heat transfer is the dominant mode of heat transfer for the total heat flux measurement as implemented in ISO 9705. The results also suggest that the total heat flux measurement, as implemented in ISO 9705, can be partitioned to infer the incident radiation with an estimated relative uncertainty of 7%–25% when the total heat flux is above 5000 $W/m^2$. Near flashover conditions, 20000 $W/m^2$, the relative uncertainty is estimated to be 7%–8%.

A total heat flux measurement is not recommended for computing incident radiation from a mixed-mode heat transfer environment with heat flux levels below 5000 $W/m^2$. For measurements of total heat flux with heat flux levels near or above 20000 $W/m^2$ and dominated by radiation, the uncertainty of the calculated incident radiation, as illustrated here, may be considered acceptable. However, characterization of the local gas flow environment around the total heat flux gauge with a temperature measurement and, at minimum, a good estimate of velocity is strongly recommended.

The uncertainty analysis demonstrates how major sources of uncertainty can be identified and evaluated to reduce the total uncertainty. Based on the model equations selected and the conditions of the example room corner surface products test, the free-stream temperature measurement and the heat flux gauge calibration constant were identified as the major sources of uncertainty. The heat flux gauge surface diameter was also identified as a parameter that can adversely affect the uncertainty estimate.

More complex measurements, such as heat flux gauges embedded in burning objects, also require uncertainty estimates and, if possible, partitioning of heat transfer modes. The present study begins to enhance the understanding of the challenges of performing such heat flux measurements accurately. Future work should focus on applying the approach described here to calculate uncertainties implicit in these more complex heat flux measurement situations. The illustrative example presented here should provide guidance on the best approach to such measurements.

## REFERENCES


1. Holmberg DG, Womeldorf CA, Grosshandler WL. *Design and Uncertainty Analysis of a Second-Generation Convective Heat Flux Calibration Facility*, vol. 4. ASME: New York, 1999; 65.
2. Holmberg DG, Womeldorf CA. *Performance and Modeling of Heat Flux Sensors in Different Environments*, vol. 4. ASME: New York, 1999; 71.
3. Robertson AF, Ohlemiller TJ. Low heat-flux measurements: some precautions. *Fire Safety Journal* 1995; **25**:109.
4. Wetterlund I, Persson B. *Calibration and Use of Heat Flux Meters*, vol. 1. Interscience Communications Ltd.: London, England, 1999; 35.
5. Taylor JR. *An Introduction to Error Analysis—The Study of Uncertainties in Physical Measurements* (2nd edn). University Science Books: Sausalito, CA, 1997; 45–79.
6. *Fire Tests—Full-Scale Room Test for Surface Products*, ISO 9705. International Organization for Standardization: Geneva, Switzerland, 1993.
7. Borell GJ, Diller TE. A convection calibration method for local heat-flux gauges. *Journal of Heat Transfer-Transactions of the ASME* 1987; **109**:83.
8. Kidd CT, Nelson CG. *How the Schmidt–Boelter Gage Really Works*, vol. 41. Instrument Society of America: Research Triangle Park, NC, 1995; 347.
9. Holman JP, Gajda WJ. *Experimental Methods for Engineers*, (4th edn), McGraw-Hill: New York, 1984; 304.
10. Arai N, Matsunami A, Churchill SW. A review of measurements of heat flux density applicable to the field of combustion. *Experimental Thermal and Fluid Science* 1996; **12**:452.
11. Bryant RA, Johnsson EL, Ohlemiller TJ, Womeldorf CA. *Estimates of the Uncertainty of Radiative Heat Flux Calculted From Total Heat Flux Measurements*, vol. 1. Interscience Communications Ltd.: London, England, 2001; 605.

12. Tsutsui T, Igarashi T, Nakamura H. Fluid flow and heat transfer around a cylindrical protuberance mounted on a flat plate boundary layer. *Japanese Society of Mechanical Engineers International Journal Series B-Fluids and Thermal Engineering* 2000; **43**:279.
13. Incropera FP, De Witt DP. *Introduction to Heat Transfer*, (2nd edn). Wiley: New York, 1990; 366.
14. *General Description of Radiant Calibration Procedures for Heat Flux Transducers and Infrared Radiometers*, MEDTHERM Procedure No. PI-20. MEDTHERM Corporation: Huntsville, AL, 1995.
15. Kline SJ. The purposes of uncertainty analysis. *Journal of Fluids Engineering Transactions of the ASME* 1985; **107**:153.
16. Kokkala M, Goransson U, Soderbom J. *Five Large-Scale Room Fire Experiments—Project 3 of the EUREFIC Fire Research Programme*, VTT 104, Technical Research Centre of Finland: Espoo, Finland, 1992.
17. Kuyatt CE, Taylor BN. *Guidelines for Evaluating and Expressing the Uncertainty of NIST Measurement Results*, NIST/TN-1297. NIST: Gaithersburg, MD, 1994.
18. Blevins LG, Pitts WM. Modeling of bare and aspirated thermocouples in compartment fires. *Fire Safety Journal* 1999; **33**:239.